

Statistical Properties of Dissipative MHD Accelerators

Kaspar Arzner¹, Loukas Vlahos², Bernard Knaepen³ and Nicolas Denewet³

¹ Paul Scherrer Institut
Laboratory for Astrophysics
CH-5232 Villigen PSI, Switzerland
arzner@astro.phys.ethz.ch

² Aristotle University
Institute of Astronomy, Dept. of Physics
54006 Thessaloniki, Greece
vlahos@astro.auth.gr

³ Université Libre de Bruxelles
Mathematical Physics Dept.
CP231, Boulevard du Triomphe
1050 Bruxelles, Belgium
bknaepen@ulb.ac.be

Abstract. We use exact orbit integration to investigate particle acceleration in a Gauss field proxy of magnetohydrodynamic (MHD) turbulence. Regions where the electric current exceeds a critical threshold are declared to be ‘dissipative’ and endowed with super-Dreicer electric field $\mathbf{E}_\Omega = \eta \mathbf{j}$. In this environment, test particles (electrons) are traced and their acceleration to relativistic energies is studied. As a main result we find that acceleration mostly takes place within the dissipation tails, and that the momentum increments have heavy (non-Gaussian) tails, while the waiting times between the dissipation regions are approximately exponentially distributed with intensity proportional to the particle velocity. No correlation between the momentum increment and the momentum itself is found. Our numerical results suggest an acceleration scenario with ballistic transport between independent ‘black box’ accelerators.

1 Introduction

Astrophysical high-energy particles manifest as cosmic rays or, indirectly, as radio waves, X-rays, Gamma rays. These often occur in transients, and with distinctly non-equilibrium energy distributions. A prominent source of sporadic radio- and X-ray emission is the Sun during the active phase of its 11-year cycle. Among the numerous mechanisms proposed for accelerating solar particles to high energies (see [1] for an overview), stochastic ones attracted particular attention because they require generic input data and do not rely on special geometrical assumptions. In stochastic acceleration [2,3,4,5], particles move

in random electromagnetic fields, where they become repeatedly deflected and, on average, accelerated. The electromagnetic fields are thought to arise from magneto-hydrodynamic (MHD) turbulence (e.g., [6]), perhaps excited by the broadband echo of a magnetic collapse. The turbulence may host shocks and other forms of dissipation if critical velocities [7] or electric current densities [8,9] are exceeded. Associated with dissipation are (collisional or anomalous) resistivity and non-conservative electric fields, which sustain, locally, the electric current against dissipative drag in order to meet the global constraints. However, a detailed balance on the level of individual charge carriers is impossible because the dissipative drag depends on particle position *and* velocity, whereas the electric field is a function of position only. Thus the electric field may compensate the bulk drag, but a (high-energy) population can be left over and exposed to acceleration [10]. This lack of detailed balance is in the heart of dissipative acceleration mechanisms. In plasmas, dissipation occurs at ‘ruptures’ of the magnetic structure, and is therefore localized around critical points of the magnetic field.

The above scenario, first envisaged by Parker [11] for the solar atmosphere, has since been explored in a large number of numerical studies [12,13,14,6,15,16,17]. On the theoretical side, most stochastic acceleration theories [2,18,19] base on Fokker-Planck approaches, thus transferring two-point functions of the electromagnetic fields into drift and diffusion coefficients of particles by probing the fields along unperturbed trajectories. Dynamical particle averages are then replaced by field ensemble averages, neglecting the fact that real particles move in *one* realization of the random field. As a result, diffusive behaviour may be predicted even if particles are trapped in a single realization of the random field.

In order to investigate the full diversity of orbit behaviour one must resort to numerical simulations. In the present contribution we analyze the behaviour of test particles in resistive MHD turbulence with localized dissipation regions, with particular emphasis on the validity of a Fokker-Planck description [20]. We use here exact orbit integration, and thus avoid any guiding centre approximations [21,22]. The price for rigorosity is computational cost, which makes the scheme only feasible with the aid of high-performance computing.

2 Acceleration Environment

The MHD turbulence has been modeled by full 3D spectral MHD simulations and by Gauss field proxies [23,17]. We concentrate here on the latter, which is computed from the vector potential $\mathbf{A}(\mathbf{x}, t) = \sum_{\mathbf{k}} \mathbf{a}_{\mathbf{k}} \cos(\mathbf{k} \cdot \mathbf{x} - \omega(\mathbf{k})t - \phi_{\mathbf{k}})$ by means of tabulated trigonometric calls. This allows to continuously determine the fields at the exact particle position, and avoids any real-space discretization artifacts, but the computational overhead restricts the \mathbf{k} sum to a few 100 Fourier modes $\mathbf{a}_{\mathbf{k}}$. They are taken from the shell $\min(l_i^{-1}) < |\mathbf{k}| < 10^{-2} r_L^{-1}$ with r_L the rms thermal ion Larmor radius and l_i the outer scale of the power spectral density $\langle |\mathbf{a}_{\mathbf{k}}|^2 \rangle \propto (1 + l_x^2 k_x^2 + l_y^2 k_y^2 + l_z^2 k_z^2)^{-\nu}$. The electromagnetic fields are then obtained from

$$\mathbf{B} = \nabla \times \mathbf{A} \quad (1)$$

$$\mathbf{E} = -\partial_t \mathbf{A} + \eta(\mathbf{j}) \mathbf{j}, \quad (2)$$

where $\mu_0 \mathbf{j} = \nabla \times \mathbf{B}$ and $\eta(\mathbf{j}) = \eta_0 \theta(|\mathbf{j}| - j_c)$ is an anomalous resistivity switched on above the critical current $j_c \sim enc_s$. Here, c_s and n are the sound speed and number density of the background plasma. The Gauss field \mathbf{A} must satisfy the MHD constraints

$$\mathbf{E} \cdot \mathbf{B} = 0 \quad \text{if} \quad \eta(\mathbf{j}) = 0 \quad \text{and} \quad E/B \sim v_A \quad (3)$$

with v_A the Alfvén velocity. Equation (3) can be achieved in several ways. For instance, one can use Euler potentials of which only one is time-dependent, or force \mathbf{A} to point along a single direction. A somewhat more flexible way, used here, is axial gauge $\mathbf{a}_\mathbf{k} \cdot \mathbf{v}_A = 0$ with dispersion relation $\omega(\mathbf{k}) = \mathbf{k} \cdot \mathbf{v}_A$. A constant magnetic field B_0 along \mathbf{v}_A can be included without violating Eq. (3), and we set $|\mathbf{v}_A|^2 = (B_0^2 + \sigma_B^2)/(\mu_0 n m_p)$ with σ_B the rms magnetic fluctuations and m_p the proton rest mass. In the present simulation, \mathbf{v}_A and the background magnetic field are along the z direction. The total magnetic field $\mathcal{B} = \sqrt{B_0^2 + \sigma_B^2}$ is a free parameter, which defines the scales of the particle orbits. In order to represent coronal turbulence we choose $v_A \sim 2 \cdot 10^6$ m/s, $\nu = 1.5$, $\mathcal{B} \sim 10^{-2}$ T, $\sigma_B = 10^{-2}$ T, $B_0 = 10^{-3}$ T, and $l_x = l_y = 10^3$ m, $l_z = 10^4$ m. The current threshold j_c is exceeded in about 7% of the total volume. Note that our choice represents strong ($\sigma_B \gg B_0$) and anisotropic ($l_z \gg l_x, l_y$) turbulence. To embed our simulation in the real solar atmosphere one should associate l_z with the radial direction in order to reproduce the predominant orientation of coronal filaments.

3 Particle Dynamics

3.1 Physical Scaling

Time is measured in units of the (non-relativistic) gyro period $\Omega^{-1} = m/q\mathcal{B}$; velocity in units of the speed of light; distance in units of $c\Omega^{-1}$. Particle momentum is measured in units of mc ; the vector potential in units of mc/q ; the magnetic field in units of \mathcal{B} ; the electric current density in units of $\Omega\mathcal{B}/(\mu_0 c)$, so that the dimensionless threshold current is $j'_c = (m/m_p)c_s c/v_A^2$; and the electric field is measured in units of $c\mathcal{B}$, so that the dimensionless Dreicer [10] field is $E'_D = (v'_e/\tau')(m_e/m)$ with v'_e the electron thermal velocity and τ' the electron-ion collision time. The dimensionless equations of motion are

$$\frac{d\mathbf{x}'}{dt'} = \mathbf{v}' \quad (4)$$

$$\frac{d(\gamma\mathbf{v}')}{dt'} = \mathbf{v}' \times \mathbf{B}' - \frac{\partial \mathbf{A}'}{\partial t} + \eta'(|\mathbf{j}'|) \mathbf{j}' \quad (5)$$

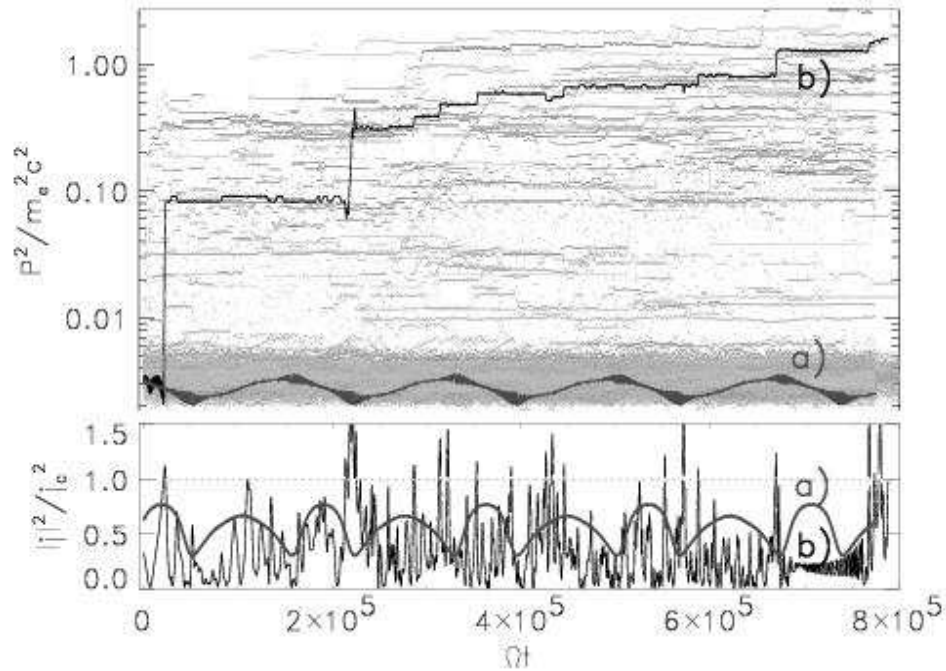


Fig. 1. Evolution of electron kinetic momentum. Top panel: 200 sample orbits; adiabatic (a), and accelerated (b) cases. Bottom panel: electric current density along the orbits a) and b). The critical current density ($|\mathbf{j}| > j_c$) is marked by dotted line. The present simulation is an extension of the simulation of [17].

with γ the Lorentz factor, $\mathbf{B}' = \nabla' \times \mathbf{A}'$, and $\mathbf{j}' = \nabla' \times \mathbf{B}'$ the electric current. The dimensionless resistivity η' is characterized by the resulting dissipative electric field $\mathbf{E}_\Omega = \eta_0 \mathbf{j}$ relative to the Dreicer field E_D . We chose η' such that $E_\Omega/E_D \sim 10^4$.

3.2 Particle Initial Conditions

We consider electrons as test particles. The initial positions are uniformly distributed in space, and the velocities are from the tail $v \geq 3 v_{th}$ of a maxwellian of 10^6 K, which is typical for the solar corona. Coulomb collisions are neglected, which is a good approximation once the acceleration has set on, but is not strictly correct in the beginning of the simulation.

3.3 Numerical Implementation and Simulation Management

Equations (4) and (5) are integrated by traditional leapfrog and Runge-Kutta schemes. The test particle code is written in FORTRAN 90/95 and compiled by

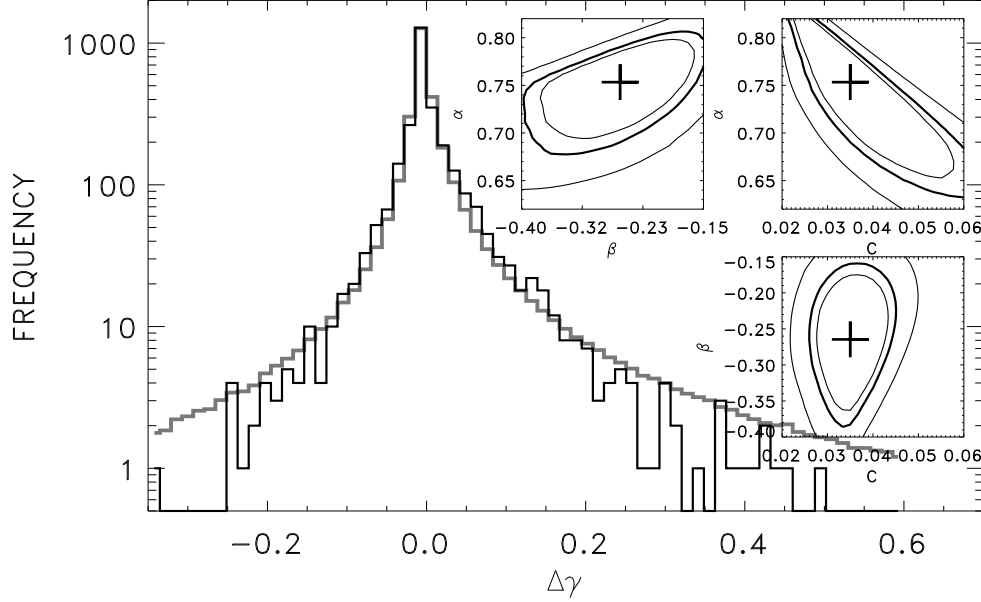


Fig. 2. Frequency distribution of the energy jumps $\Delta\gamma$ of Fig. 1 (black line), together with a best-fit Lévy density (gray line) with parameters $\alpha_0 = 0.75$, $\beta_0 = -0.26$, and $C_0 = 0.035$ (crosses). Inlets: cuts of the likelihood surface at (α_0, β_0, C_0) . The 99% confidence level is marked boldface.

the Portland Group's Fortran 90 compiler (**pgf90**). Diagnostics and visualization uses IDL as a graphical back-end. The code is run on the MERLIN cluster of the Paul Scherrer Institut, and on the ANIC-2 cluster of the Université libre de Bruxelles. The ANIC-2 cluster has 32 single Pentium IV nodes, a total of 48 Gbyte memory, and Ethernet connections. The MERLIN cluster consist of 56 mostly dual Athlon nodes with a total of 80 GByte memory, operated under Linux and connected by Myrinet and Ethernet links. MERLIN jobs are managed by the Load Sharing Facility (LSF) queueing system. Parallelization is done on a low level only, with different (and independent) test particles assigned to different CPU's. MPICH/MPI is used to ensure crosstalk-free file I/O. The field data are computed on each CPU for the actual particle position. Random numbers are needed in the generation of the Fourier amplitudes and -phases of the electromagnetic fields, and in the particle initial data; they are taken from the intrinsic random number generator of **pgf90**.

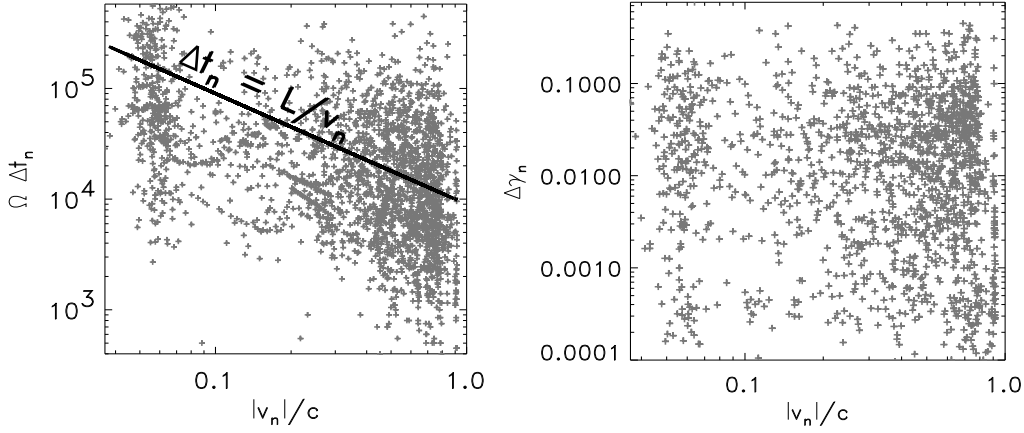


Fig. 3. Left: travel times $\Delta t_n = t_{n+1} - t_n$ between acceleration regions versus velocity v_n . Right: energy gain $\Delta\gamma_n = \gamma_{n+1} - \gamma_n$ versus velocity. While Δt_n scales with inverse velocity (solid line: best-fit), there is no clear trend in the energy gain $\Delta\gamma_n$.

4 Diagnostics and Results

In order to characterize the relativistic acceleration process we consider the evolution of the kinetic momentum $\mathbf{P}' = \gamma\mathbf{v}'$. This quantity is directly incremented by the equation of motion (5), and – ignoring quantum effects – can grow to arbitrarily large values, so that it can serve as a diagnostics of diffusive behaviour. Alternatively we may use the kinetic energy γ .

The results of the orbit simulations are shown in Figs. 1 - 4. When initially super-thermal ($v \gtrsim 3v_{th}$) electrons move in the turbulent electromagnetic fields (Eqns. 1, 2), some of them may become stochastically accelerated. From a population of 600 electrons we find that 35% of the particles are accelerated, while the other 65% remain adiabatic [22,24] during the simulation ($\Omega t \leq 8 \cdot 10^5$). The two cases are illustrated in Fig. 1 (top). The orbit a) conserves energy adiabatically during the whole simulation, while the orbit b) does not. The orbits of 200 randomly chosen particles are also shown (gray) to trace out the full population. The bottom panel of Fig. 1 shows the electric current density along the orbits a) and b). Time intervals where the critical current (dotted line) is exceeded correspond to visits to the dissipation regions. As can be seen, acceleration (or deceleration) occurs predominantly within the dissipation regions. Accordingly, the orbit b) which never enters a dissipation region remains adiabatic. As a benchmark we have set $\eta_0 = 0$ and found that no acceleration takes place at all, thus reproducing the ‘injection problem’ [25]. Smaller η' yield smaller (than 35%) fractions of accelerated particles.

A glance at graph a) of Fig. 1 shows that $\mathbf{P}'(t')$ is poorly represented by a Brownian motion [20] with continuous sample paths. Rather, \mathbf{P}' changes

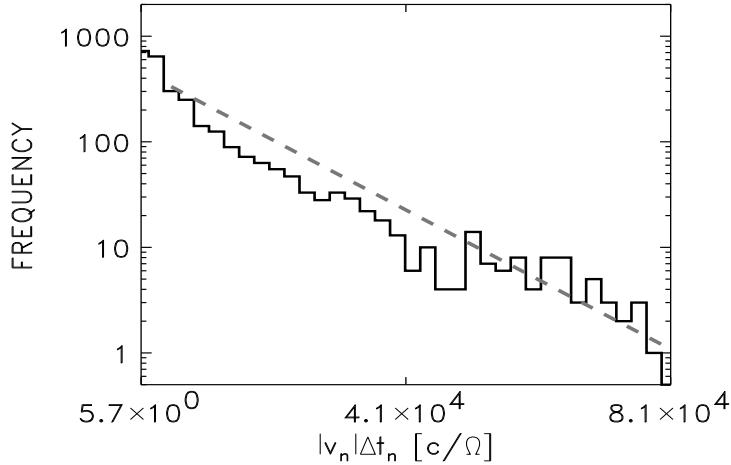


Fig. 4. Histogram of the quantity $|v_n|\Delta t_n$, together with an exponential fit (dashed).

intermittently and in large jumps. Indeed, if we consider the energy change $\Delta\gamma_n = \gamma_{n+1} - \gamma_n$ across a dissipation region, we find that its distribution $P(\Delta\gamma_n)$ has heavy tails and a convex shape which deviates from a Gaussian law (Fig. 2 black line). In order to characterize $P(\Delta\gamma_n)$ we have tried to fit it by a (skew) Lévy stable distribution $P_L(x)$. The latter is defined in terms of its Fourier transform [26]

$$\phi_L(s) = \exp \left\{ -C|s|^\alpha \left(1 + i\beta \frac{s}{|s|} \tan \frac{\pi\alpha}{2} \right) \right\} \quad (6)$$

with $0 < \alpha \leq 2$, $-1 \leq \beta \leq 1$, and $C > 0$. The parameter α determines the asymptotic decay of $P_L(x) \sim x^{-1-\alpha}$ at $x \gg C^{1/\alpha}$, and β determines its skewness. The probability density function (PDF) belonging to Eq. (6) has the ‘stability’ property that the sum of independent identically Lévy distributed variates is Lévy distributed as well. While rapidly converging series expansions [26] of $P_L(x)$ are available for $1 < \alpha \leq 2$ or large arguments x , the evaluation of $P_L(x)$ at small arguments and $\alpha < 1$ is more involved. We use here a strategy where $P_L(x)$ is obtained from direct computation of the Fourier inverse $P_L(x) = (2\pi)^{-1} \int e^{-isx} \phi_L(s) ds$, with the integrand split into regimes of different approximations. At small $|s|$, both the exponential in $\phi_L(s)$ (Eq. 6) and the Fourier factor e^{-isx} are expanded; at larger $|s|$, $\phi_L(s)$ is piecewise expanded while e^{-isx} is retained. In both cases, the s -integration can be done analytically, and the pieces are summed numerically. The resulting (Poisson) maximum-likelihood estimates of the parameters (α, β, C) are $\alpha_0 = 0.75$, $\beta_0 = -0.26$, $C_0 = 0.035$. The predicted frequencies are shown in Fig. 2 (gray line), and inlets represent

sections of constant likelihood in (α, β, C) -space, with the 99% confidence region enclosed by boldface line. The finding $\alpha_0 < 2$ agrees with the presence of large momentum jumps.

In a next step we have investigated the waiting times $\Delta t_n = t_{n+1} - t_n$ between subsequent encounters with the dissipation regions. Simple ballistic transport between randomly positioned dissipation regions would predict a PDF of the form $f(|v_n| \Delta t_n)$ with v_n the particle velocity and $f(x)$ the PDF of distances between (magnetically connected) dissipation regions. (There is no Jacobian $d(\Delta t)/dx$ since we are dealing with discrete events.) This is in fact the case. Figure 3 (left) shows a scatter plot of the actual velocity v_n versus waiting time Δt_n . Gray crosses represent all simulated encounters with dissipation regions, including all particles and all simulated times. There is a clear trend for Δt_n to scale with v_n^{-1} , and the black solid line represents a best fit of the form $\Delta t_n = L/v_n$ with $L = 9 \cdot 20^3 c/\Omega$. When a similar scatter plot of velocity versus energy gain is created (Fig. 3 right), then no clear correlation is seen: the energy gain is apparently independent of energy. In this sense the dissipation regions ‘erase’ the memory of the incoming particles. Returning to the waiting times, we may ask for the shape of the function $f(|v_n| \Delta t_n)$. This can be determined from a histogram of the quantity $|v_n| \Delta t_n$ (Fig. 4, solid line). The decay is roughly exponential (dashed: best-fit), although the limited statistics does certainly not allow to exclude other forms.

5 Summary and Discussion

We have performed exact orbit integrations of electrons in a Gauss field proxy of MHD turbulence with super-Dreicer electric fields localized in dissipation regions. It was found that the electrons remain adiabatic (during the duration of the simulation) if no dissipation regions are encountered, and can become accelerated if such are met. The resulting acceleration is intermittent and is not well described by a diffusion process, even if the underlying electromagnetic fields are Gaussian. On time scales which are large compared to the gyro time, the kinetic momentum performs a Lévy flight rather than a classical Brownian motion. The net momentum increments in the dissipation regions are independent of the incoming momentum, and have heavy tails which may be approximated by a stable law of index 0.75. The waiting times between subsequent encounters with dissipation regions are approximately exponentially distributed, $P(\Delta t) \sim e^{-v\Delta t/L}$, indicating that the dissipation regions are randomly placed along the magnetic field lines. This one-dimensional Poisson behaviour is most likely caused by the Gauss field approximation, and the waiting times in true MHD turbulence are expected to behave differently. An ongoing study is devoted to these questions, and results will be reported elsewhere. In summary, our numerical results suggest that the acceleration process may be modeled by a continuous-time random walk with finite or infinite mean waiting time, and infinite variance of the momentum increments. Such models can be described in terms of fractional versions [27,28] of the Fokker-Planck equation.

References

1. Miller, J., Cargill, P. J., Emslie, A. G., Holman, G. D. Dennis, B. R., LaRosa, T. N., Winglee, R. M., Benka, S. G., Tsuneta, S., 1997, *J. Geophys. Res.*, 102, 14.631
2. Karimabadi, Menyuk, C.R., Sprangle, P., & Vlahos, L. 1987, *Astrophys. J.*, 316, 462
3. Miller J., & R. Ramaty, 1987, *Solar Phys.*, 113, 195
4. Miller J., LaRosa, T.N., & Melrose, R. L., 1996, *Astrophys. J.*, 461, 445
5. Miller, J., J.A., 1997, *Astrophys. J.*, 491, 939
6. Biskamp, D., & Müller, W.C., 2000, *Phys. Plasmas*, 7, 4889
7. Treumann, R., and Baumjohann, W., 1997, *Basic Space Plasma Physics*, Imperial College Press
8. Papadopoulos, K. 1997, in: *Dynamics of the Magnetosphere*, ed. Akasofu & Reidel, Dordrecht
9. Parker, E. N., 1993, *Astrophys. J.*, 414, 389
10. Dreicer, H. 1960, *Phys. Rev.*, 117, 329
11. Parker, E. N., 1983, *Astrophys. J.*, 264, 635
12. Matthaeus, W.H. & Lamkin, S.L., 1986, *Phys. Fluids*, 29, 2513
13. Ambrosiano, J., Matthaeus, W.H., Goldstein, M.L., and Plante, D., 1988, *J. Geophys. Res.*, 93, 14.383
14. Anastasiadis, A., Vlahos, L., & Georgoulis, M. K., 1997 *Astrophys. J.*, 489, 367
15. Dimitruk, P., Matthaeus, W.H., Seenu, N., & Brown, M.R. 2003, *Astrophys. J. Lett.*, 597, L81
16. Moriyashu, S., Kudoh, T., Yokoyama, T., Shibata, K., 2004, *Astrophys. J.*, 601, L107
17. Arzner, K., and Vlahos, L., 2004, *Astrophys. J. Lett.*, 605, L69
18. Karimabadi, H. N. Omid, & C.R. Menyuk 1990, *Phys. Fluids B*, 2, 606
19. Schlickeiser R. 2002, *Cosmic Ray Astrophysics*, Berlin, Springer
20. Gardiner C. W. 1985, *Handbook of stochastic methods*, Springer.
21. Littlejohn, R. G., 1982, *J. Math. Phys.*, 23(5), 742
22. Littlejohn, R. G., 1983, *J. Plasma Physics*, 29, 111
23. Adler, R. J., 1981, *The Geometry of Random Fields*, John Wiley & Sons
24. Büchner, J., and Zelenyi, L. M., 1989, *J. Geophys. Res.*, 94, 11.821
25. Cargill, P. J., 2001, in: *Encyclopedia of Astronomy and Astrophysics – Solar flares: Particle Acceleration Mechanisms*, Nature Publ. Group, IOPP, Bristol, UK
26. Lukacs, E., 1960, *Characteristic Functions*, Charles Griffin, London
27. Uchaikin, V. V., 2000 *Int. J. of Theoretical Physics*, 39, no 8, 2087
28. Meerschaert M. M. and Benson, D. A., 2002, *Phys. Rev. E*, 66, 060102(R)